## Deformation and Collectivity in Doubly Magic <sup>208</sup>Pb

```
J. Henderson<sup>®</sup>, <sup>1,*</sup> J. Heery<sup>®</sup>, <sup>1</sup> M. Rocchini<sup>®</sup>, <sup>2,3</sup> M. Siciliano<sup>®</sup>, <sup>4</sup> N. Sensharma<sup>®</sup>, <sup>4</sup> A. D. Ayangeakaa<sup>®</sup>, <sup>5,6</sup>
R. V. F. Janssens, 5,6 T. M. Kowalewski, 5,6 Abhishek, P. D. Stevenson, E. Yüksel, B. A. Brown, 7,8 T. R. Rodriguez, 9,10,11 L. M. Robledo, 10,11,12 C. Y. Wu, 13 S. Kisyov, 13,† C. Müller-Gatermann, V. Bildstein, L. Canete, C. M. Campbell, A. Carmichael, S. Carmichael, S. Kisyov, L. Carpenter, W. N. Catford, P. Copp, 4,‡ C. Cousins, M. Devlin, D. T. Doherty, P. E. Garrett, U. Gargo, L. P. Gaffney, T. K. Hadynska-Klek, B. D. J. Hartley, S. F. Hicks, 20,21 H. Jayatissa, 4,‡ S. R. Johnson, 5,6 D. Kalaydjieva, P. F. Kondev, D. Lascar, 23 T. Lauritsen, G. Lotay, N. Marchini, M. Matejska-Minda, A. Radich, R. Rathod, S. R. Rathod, S. P. H. Regan, 1,25 C. J. Paxman, A. Perkoff, E. E. Peters, 20 Zs. Podolyák, A. Radich, R. Rathod, S. R. Rathod, S. J. Reedo, S. P. H. Regan, 1,27 W. Reviol, 4 E. Pubino, 7,1 P. Puscall, D. Savarynick, J. P. Varboy, A. P. Wilson, 428,1
                              E. Rubino, <sup>7,||</sup> R. Russell<sup>0</sup>, <sup>1</sup> D. Seweryniak, <sup>4</sup> J. R. Vanhoy, <sup>19</sup> G. L. Wilson<sup>0</sup>, <sup>4,28</sup>, <sup>1</sup> K. Wrzosek-Lipska<sup>0</sup>, <sup>18</sup> S. W. Yates, <sup>20</sup> and I. Zanon<sup>0</sup>
                       <sup>1</sup>School of Mathematics and Physics, University of Surrey, Guildford GU2 7XH, United Kingdom
                      <sup>2</sup>Istituto Nazionale di Fisica Nucleare, Sezione di Firenze, I-50019 Sesto Fiorentino (Firenze), Italy
                                  <sup>3</sup>Department of Physics, University of Guelph, Guelph, Ontario N1G2W1, Canada
                                                  <sup>4</sup>Argonne National Laboratory, Lemont, Illinois 60439, USA
                                         <sup>5</sup>University of North Carolina, Chapel Hill, North Carolina 27599, USA
                      <sup>6</sup>Triangle Universities Nuclear Laboratory, Duke University, Durham, North Carolina 27708, USA
                      <sup>7</sup>Facility for Rare Isotope Beams, Michigan State University, East Lansing, Michigan 48824, USA
                   <sup>8</sup>Department of Physics & Astronomy, Michigan State University, East Lansing, Michigan 48824, USA
            <sup>9</sup>Departamento de Estructura de la Materia, Física Térmica y Electrónica, Universidad Complutense de Madrid,
                                                                            E-28040 Madrid, Spain
                         <sup>10</sup>Departamento de Física Teórica, Universidad Autónoma de Madrid, E-28049 Madrid, Spain
                       <sup>11</sup>Centro de Investigación Avanzada en Física Fundamental-CIAFF-UAM, E-28049 Madrid, Spain
                   <sup>12</sup>Center for Computational Simulation, Universidad Politécnica de Madrid, Campus de Montegancedo,
                                                            Bohadilla del Monte, E-28660 Madrid, Spain
                                    <sup>13</sup>Lawrence Livermore National Laboratory, Livermore, California 94550, USA
                   <sup>14</sup>Nuclear Science Division, Lawrence Berkeley National Laboratory, Berkeley, California 94720, USA
         <sup>15</sup>Department of Physics and Astronomy and The Joint Institute for Nuclear Astrophysics, University of Notre Dame,
                                                                  30 Notre Dame, Indiana 46556, USA
                                       <sup>16</sup>Los Alamos National Laboratory, Los Alamos, New Mexico 87545, USA
                                      <sup>17</sup>Department of Physics, University of Liverpool, Liverpool, United Kingdom
                                      <sup>18</sup>Heavy Ion Laboratory, University of Warsaw, PL-02-093 Warsaw, Poland
                                  <sup>19</sup>Department of Physics, U.S. Naval Academy, Annapolis, Maryland 21402, USA
            <sup>20</sup>Departments of Chemistry and Physics & Astronomy, University of Kentucky, Lexington, Kentucky 40506, USA
                                         <sup>21</sup>Department of Physics, University of Dallas, Irving, Texas 75062, USA
                                                      <sup>22</sup>IRFU, CEA Saclay, Université Paris-Saclay, France
                       <sup>23</sup>Department of Physics and Astronomy, Northwestern University, Evanston, Illinois 60208, USA
                                       <sup>24</sup>Institute of Nuclear Physics Polish Academy of Sciences, Kraków, Poland
                      <sup>25</sup>National Institute for Physics and Nuclear Engineering, Bucharest-Magurele, R-77125, Romania <sup>26</sup>U.S. Naval Academy, Annapolis, Maryland 21402, USA
                                <sup>27</sup>National Physical Laboratory, Teddington, Middlesex TW11 OLW, United Kingdom
                 <sup>28</sup>Department of Physics and Astronomy, Louisiana State University, Baton Rouge, Louisiana 70803, USA
                                 <sup>29</sup>Laboratori Nazionali di Legnaro, Laboratori Nazionali di Legnaro, Legnaro, Italy
```

(Received 5 July 2024; revised 3 October 2024; accepted 18 December 2024; published 14 February 2025)

Published by the American Physical Society under the terms of the Creative Commons Attribution 4.0 International license. Further distribution of this work must maintain attribution to the author(s) and the published article's title, journal citation, and DOI.

<sup>\*</sup>Contact author: jack.henderson@surrey.ac.uk

<sup>&</sup>lt;sup>†</sup>Present address: Nuclear Science Division, Lawrence Berkeley National Laboratory, Berkeley, California 94720, USA.

<sup>&</sup>lt;sup>‡</sup>Present address: Los Alamos National Laboratory, Los Alamos, New Mexico 87545, USA.

<sup>§</sup>Present address: TRIUMF, Vancouver V6T 2A3, British Columbia, Canada.

Present address: Lawrence Livermore National Laboratory, Livermore, California 94550, USA.

Present address: UK Atomic Energy Authority, Culham Campus, Abingdon OX14 3DB, United Kingdom.

Lead-208 is the heaviest known doubly magic nucleus and its structure is therefore of special interest. Despite this magicity, which acts to provide a strong restorative force toward sphericity, it is known to exhibit both strong octupole correlations and some of the strongest quadrupole collectivity observed in doubly magic systems. In this Letter, we employ state-of-the-art experimental equipment to conclusively demonstrate, through four Coulomb-excitation measurements, the presence of a large, negative, spectroscopic quadrupole moment for both the vibrational octupole  $3^-_1$  and quadrupole  $2^+_1$  state, indicative of a preference for prolate deformation of the states. The observed quadrupole moment is discussed in the context of the expected splitting of the  $3^- \otimes 3^-$  two-phonon states, due to the coupling of the quadrupole and octupole motion. These results are compared with theoretical values from three different methods, which are unable to reproduce both the sign and magnitude of this deformation. Thus, in spite of its well-studied nature,  $2^{08}$ Pb remains a puzzle for our understanding of nuclear structure.

DOI: 10.1103/PhysRevLett.134.062502

Since the identification of the nuclear spin-orbit interaction, and its role in the creation of so-called magic numbers [1,2], doubly magic nuclei have acted as cornerstones of nuclear physics. These isotopes act to delimit the nuclear landscape, allowing it to be subdivided into relatively manageable valence spaces. Of these key isotopes, <sup>208</sup>Pb is the heaviest known example, lying at the intersection of the proton Z = 82 and neutron N = 126magic numbers that dictate the nuclear structure of the mass region (see, e.g., Refs. [3.4]). Studying this nucleus is thus key to understanding not only the structure of doubly magic nuclei, but also the entire region of the nuclear landscape around mass number A = 200 with broad implications. For example, the aforementioned N = 126 magic number plays a critical role in the formation of the third abundance peak of the astrophysical r process—a series of rapid neutron captures leading to the formation of approximately half of the elements heavier than iron in our Galaxy. Specifically, the intersection of the r process capture path with the N = 126 shell closure results in an accumulation of material in the  $A \sim 195$  region [5], producing a broad peak in the observed abundance pattern of many stars in the Milky Way. Given that this is one of the key signatures of "main" r-process nucleosynthesis, understanding the properties of nuclei in this region is of paramount importance for our understanding of the production of heavy elements. Beyond the role the N = 126 shell closure plays in r-process nucleosynthesis, <sup>208</sup>Pb is also key to the determination of the symmetry energy, J, and its slope, L, in the nuclear equation of state, which governs the properties of nuclear matter under extreme conditions, such as those found in neutron stars. The neutron-skin thickness of <sup>208</sup>Pb has been experimentally investigated using parity-violating electron scattering [6,7], hadronic [8,9], electroweak [10], and gravitational wave [11] probes. Because of the strong correlation between this nuclear property and L, it has been possible to place constraints on the nuclear equation of state around saturation densities [12,13] as well as on the maximum neutron star mass radius [14]. Key to this, however, is a detailed knowledge of the structure of <sup>208</sup>Pb, which lies at the frontier of state-of-the-art *ab initio* nuclear theory [15].

The nuclear magic numbers act to stabilize spherical nuclear configurations, whereas collective properties emerge naturally from the deviation of the nucleus from sphericity. Any distinction is, however, somewhat contrived, as evidenced by the existence of shape coexistence in doubly magic systems (see, e.g., Ref. [16]). The nucleus is not a rigid object, with a broad ("soft") minimum in its potential energy surface with respect to deformation, allowing for its collective wave function to have some distribution in deformation parameter space [17]. Collective observables typically relate to the square of the nuclear collective wave function and any softness in deformation space introduces a collective behavior, even if the nucleus itself exhibits a spherical minimum in its potential energy. Indeed, these oscillations about sphericity have led to recent assertions that the very meaning of a nuclear shape for doubly magic nuclei is to be treated with caution [17].

Arguably the most famous example of a vibrational excitation in nuclear physics is the 3<sup>1</sup>/<sub>1</sub> state in <sup>208</sup>Pb [18]. This state is unusual in many senses, not least as a rare example of a first-excited state in an even-even nucleus that is not  $J^{\pi} = 2^+$ . The presence of a 3<sup>-</sup> state at low excitation energy in an even-even nucleus is indicative of a relatively strong degree of octupole collectivity, further borne out by experiment, with a  $B(E3; 3_1^- \rightarrow 0_1^+)$  transition strength of 33.8(6) W.u. [19]. Nonetheless, <sup>208</sup>Pb remains a doubly magic system, resistant to any permanent deformation in its ground state, and this excitation is thus thought to be vibrational. As a one-phonon octupole vibration, this state is expected to be accompanied by a quartet of  $3^- \otimes 3^-$  twophonon partners, with  $J^{\pi}=0^+,2^+,4^+,6^+$ , lying at approximately twice its energy. The location and splitting of this quartet is, however, strongly influenced by the coupling of the octupole and quadrupole motion in the system [20–22]. To date, this quartet of two-phonon states has eluded conclusive identification [23], with the best evidence presented for the  $0^+$  member [24,25], raising questions about the potential strength of this quadrupole coupling.

Our understanding of the couplings of the quadrupole and octupole motions, and the quadrupole behavior of the nucleus more generally, is aided by the study of three experimental observables: the transition strength between the  $2_1^+$  excited state and the  $0_1^+$  ground state  $(B(E2; 2_1^+ \rightarrow 0_1^+))$ , and the spectroscopic quadrupole moments  $(Q_s)$  of the  $3^-_1$  and  $2^+_1$  states. Of these, the  $B(E2; 2^+_1 \to 0^+_1)$  value in <sup>208</sup>Pb has been well measured, and is found to be 8.3(5) W.u., which is considerably smaller than expected for a nucleus exhibiting permanent deformation (i.e., a rotor), but is also the largest value observed for any doubly magic system [26]. The  $Q_s(3_1^-)$ value has also been measured [22,27–29] previously, albeit with some concern raised for the early results [27] regarding the contribution of nuclear interference terms. A careful analysis, excluding such terms, was performed in Refs. [22,29], and demonstrated a large, negative quadrupole moment,  $Q_s(3_1^-) = -0.34(15)$  e b, inconsistent with, although with a large uncertainty, theoretical descriptions available at the time. In the same work, a measurement of  $Q_s(2_1^+) = -0.7(3)$  e b was also made, with very large uncertainties. In this Letter, we present new results using a state-of-the-art experimental setup, making use of heavyion induced Coulomb excitation, demonstrating conclusively a significant role for quadrupole deformation in <sup>208</sup>Pb. We discuss these results within the context of stateof-the-art nuclear theory, finding that the observed deformation cannot be reproduced. Finally, we present the anticipated scale of the splitting of the  $3^- \otimes 3^-$  two-phonon states due to the coupling of octupole and quadrupole motion.

Excited states in <sup>208</sup>Pb were populated in heavy-ion induced Coulomb excitation by beams of <sup>70</sup>Ge (297 MeV), <sup>130</sup>Te (527 MeV), <sup>150</sup>Nd (640 MeV), and <sup>166</sup>Er (749 MeV), that impinged upon 99.86-% enriched, 0.45-mg/cm<sup>2</sup> thick <sup>208</sup>Pb targets. The Pb was deposited upon a 40-μg/cm<sup>2</sup> carbon backing, and the target was oriented with the backing facing the upstream direction. For the scattering angles used in the analysis the beam energies used correspond to distances of closest approach of more than 6 fm, sufficient to almost completely suppress any nuclear component to the excitation process [30]. Deexciting  $\gamma$ -rays were detected in the GRETINA array of high-purity germanium detectors [31], consisting of 12 modules at the time of the experiments. The relative efficiency of the GRETINA array was verified experimentally for energies up to 4806 keV using a source of <sup>66</sup>Ga alongside standard  $\gamma$ -ray calibration sources. Scattered beamlike and targetlike nuclei were detected simultaneously using the CHICO2 [32] array of 20 parallel-plate avalanche counters, with the beam and target nuclei distinguished based on their relative time of flight and scattering angle. This combined setup provides exceptional efficiency, angular resolution, and high-rate capabilities. Compared to a single-beam analysis,

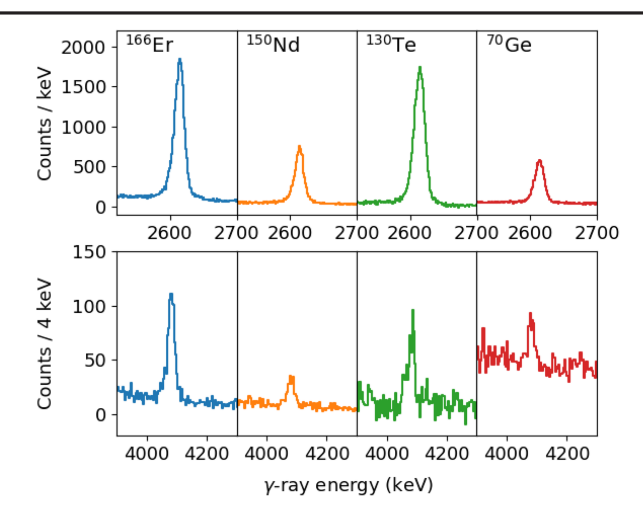


FIG. 1. Total, angle-integrated  $\gamma$ -ray spectra, Doppler-corrected for  $^{208}\text{Pb}$  reaction kinematics, showing the 2614-keV  $3_1^- \rightarrow 0_1^+$  transition [top] and the 4085-keV  $2_1^+ \rightarrow 0_1^+$  [bottom] transition for beams of  $^{166}\text{Er},~^{150}\text{Nd},~^{130}\text{Te},$  and  $^{70}\text{Ge}.$ 

a combined analysis enhances sensitivity through the use of beams of differing Z and with differing angular coverage in the center-of-mass frame. Both of these variables influence the strength of multistep Coulomb excitation and the reorientation effect, improving sensitivity to observables associated with those effects, such as spectroscopic quadrupole moments.

Gamma rays detected in GRETINA were Doppler-corrected for <sup>208</sup>Pb recoils on the basis of two-body reaction kinematics deduced from the measured scattering angle in CHICO2. Figure 1 shows two portions of the resultant Doppler-corrected γ-ray spectrum with clear peaks corresponding to the  $3_1^- \rightarrow 0_1^+$  and  $2_1^+ \rightarrow 0_1^+$  deexciting transitions at 2614 and 4085 keV, respectively. A time-random subtraction was performed to remove contributions to the 2614-keV peak due to natural background. This subtraction was validated by observing the complete removal of the 1461-keV  $\gamma$ -ray from the decay of  $^{40}$ K from the spectra. In order to enhance sensitivity to the spectroscopic quadrupole moment, the data were subdivided by the angle measured in CHICO2, allowing for the angular distribution of the reaction cross section to be assessed. Eight angular ranges were used for the data acquired with <sup>166</sup>Er and <sup>150</sup>Nd beams, and four angular ranges each for the <sup>130</sup>Te and <sup>70</sup>Ge data. The size, location, and number of angular ranges was partly dictated by the reaction kinematics and the statistics of the  $2_1^+ \rightarrow 0_1^+$  transition but also so as to avoid any discontinuities in the angular distribution, or any regions where the shape of the partner nucleus (i.e., <sup>166</sup>Er, <sup>150</sup>Nd, <sup>70</sup>Ge, and <sup>130</sup>Te) excitation angular distribution deviated significantly from expectations. This allowed the use of a single, common normalization parameter for each beam for all angular ranges.

Gamma-ray yields for each angular range (see Supplemental Material) were analyzed using the GOSIA

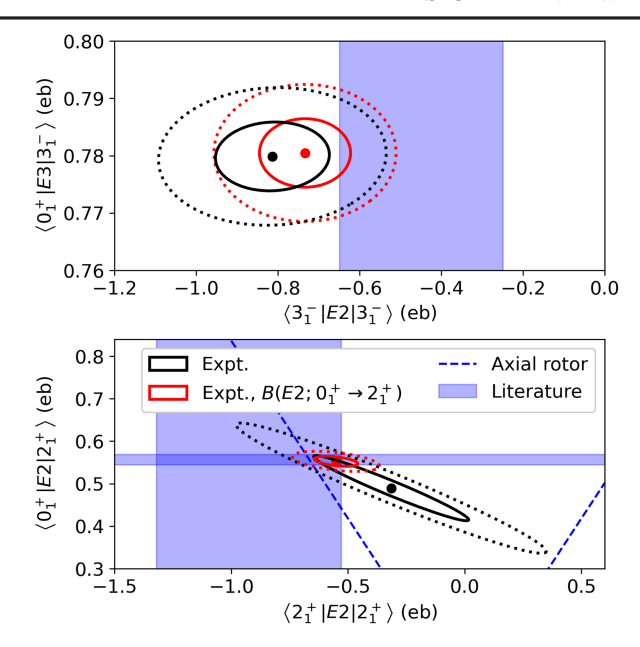


FIG. 2. Mean values (points) and confidence regions corresponding to  $1\sigma$  (solid lines) and  $2\sigma$  (dotted lines) for the  $\langle 0_1^+|E3|3_1^-\rangle$  and  $\langle 3_1^-|E2|3_1^-\rangle$  matrix elements (top), and the  $\langle 0_1^+|E2|2_1^+\rangle$  and  $\langle 2_1^+|E2|2_1^+\rangle$  matrix elements (bottom). All data were constrained by the known  $B(E3;3_1^-\to 0_1^+)=33.8(6)$  W.u. [19] strength. Limits are shown for the case where  $B(E2;2_1^+\to 0_1^+)=8.3(5)$  W.u. [40,41] was (red) and was not (black) included as a constraint in the minimization. Also shown are bands corresponding to the  $1\sigma$  limits on literature values for the  $\langle 3_1^-|E2|3_1^-\rangle$ ,  $\langle 0_1^+|E2|2_1^+\rangle$ , and  $\langle 2_1^+|E2|2_1^+\rangle$  matrix elements. Shown by the dashed line is the axial-rotor limit for the  $\langle 2_1^+|E2|2_1^+\rangle$  matrix element as a function of  $\langle 0_1^+|E2|2_1^+\rangle$ .

semiclassical Coulomb-excitation code [33], with minimization handled through an external program [34]. Data from each beam were analyzed independently to confirm consistency before a simultaneous analysis of all the data was performed. A summary of the modern Coulombexcitation analysis procedures used in this work can be found in Ref. [35]. Four parameters were varied in fitting the experimental data:  $\langle 0_1^+|E3|3_1^- \rangle$ ,  $\langle 3_1^-|E2|3_1^- \rangle$ ,  $\langle 0_1^+|E2|2_1^+ \rangle$  and  $\langle 2_1^+|E2|2_1^+\rangle$  matrix elements. The literature  $B(E3;3_1^-\rightarrow 0_1^+)$ value [18,22] and its uncertainty was included in the  $\chi^2$ minimisation as an additional constraint, allowing for the determination of absolute E2 and E3 matrix elements. Only the  $3^- \rightarrow 0_1^+$  and  $2_1^+ \rightarrow 0_1^+$  transitions were observed in the present work, however a comprehensive level scheme (see Supplemental Material [36]) was included in the GOSIA simulation, including the E1 transition coupling the two states of interest. The resulting confidence intervals are given in black in Fig. 2, indicating the strong correlations between the transitional  $\langle 0_1^+|E2|2_1^+\rangle$  and diagonal  $\langle 2_1^+|E2|2_1^+\rangle$  matrix elements. To better constrain  $\langle 2_1^+|E2|2_1^+\rangle$ , the  $B(E2;2_1^+\to$  $0_1^+$ ) strength was included as an additional datum [40,41], resulting in the more tightly constrained confidence intervals shown in red in Fig. 2. The resulting values are presented in

TABLE I. Transition and diagonal E2 and E3 matrix elements determined from an analysis combining all data obtained in the present work. Where indicated, the literature  $B(E2; 2_1^+ \rightarrow 0_1^+)$  value was included to further constrain the minimization. Note that, in all cases, the literature  $B(E3; 3_1^- \rightarrow 0_1^+)$  strength was included as a constraint.

$J_i^{\pi}  o J_f^{\pi}$	$\langle J_i^{\pi} E2 J_f^{\pi}\rangle$ ( <i>e</i> b)	$B(E2)\downarrow$ (W.u.)	Note
$0_1^+ \to 2_1^+$	0.489(77)	6.5(21)	
$\overline{J_i^\pi}$	$\langle J_i^{\pi} E2 J_i^{\pi}\rangle$ (e b)	$Q_s(J_i^\pi)$ (e b)	Note
3 <sub>1</sub> 3 <sub>1</sub> 2 <sub>1</sub> <sup>+</sup>	-0.81(14) -0.73(11) -0.31(33)	-0.63(11) -0.57(9) -0.24(25)	B(E2) incl.
$2_{1}^{+}$	-0.55(9)	-0.42(7)	B(E2) incl.

Table I both with and without the inclusion of the literature  $B(E2; 2_1^+ \rightarrow 0_1^+)$  value in the fitting routine.

The results in Table I are presented alongside the reduced transition strengths  $[B(E\lambda)]$  in Weisskopf units (W.u.), indicating the expected strength of a single-particle transition.  $B(E\lambda)$  values far in excess of 1 W.u. are indicative of a collective enhancement due to deformation. The results therefore paint a picture of a system with relatively strong octupole deformation, coupled to a modest quadrupole deformation, with a large spectroscopic quadrupole moment approaching the limit of an axial rotor [20] in the case of the 2<sup>+</sup> state (Fig. 2). In order to better understand these results, we compare them to new predictions from three theoretical models: the nuclear shell model, a Gogny density functional theory coupled to a symmetry-conserving configurationmixing method (SCCM), the self-consistent Hartree Fock (HF) + random-phase approximation (RPA) method, and the time-dependent Hartree-Fock (TDHF) method, using Skyrme interactions in both cases. We also compare the results to predictions from a previous theoretical study using a generator coordinate method with a relativistic energy density functional [42]. Details of the new calculations performed in this work are included in the Supplemental Material [36].

Shell-model calculations were performed using the method outlined in Ref. [43]. Particle-hole excitations are only permitted at the 1p-1h and 2p-2h level. The excitation energy of the  $2_1^+$  state in  $^{208}\text{Pb}$  in these calculations is overpredicted by approximately 700 keV and that of the  $3_1^-$  state by approximately 400 keV. The E3 values are calculated with effective charges of  $e_p=1.6$  and  $e_n=0.6$  and E2 values with  $e_p=1.5$  and  $e_n=0.98$  [44]. These shell-model calculations yield  $B(E3;3_1^-\to0_1^+)=36$  W.u. and  $B(E2;2_1^+\to0_1^+)=3.8$  W.u., with  $Q_s(3_1^-)=-0.12$  e b and  $Q_s(2_1^+)=0.08$  e b. While the experimental  $B(E3;3_1^-\to0_1^+)$  value is well reproduced, all electric-quadrupole observables are significantly underpredicted.

Of particular interest, the magnitudes of the computed  $Q_s(3_1^-)$  and  $Q_s(2_1^+)$  values are not only considerably smaller than the experimental ones, but also have opposing signs, whereas the experimental values are both negative and of comparable magnitude.

Symmetry-conserving configuration-mixing calculations were performed using the method outlined in Ref. [45]. In general, excitation energies are poorly reproduced, with  $E(3_1^-) = 5.6 \text{ MeV}$  [experiment:  $E(3_1^-) = 2.6 \text{ MeV}$ ] and  $E(2_1^+) = 9.2 \text{ MeV [experiment: } E(2_1^+) = 4.1 \text{ MeV]}.$  This is thought to be due to an as-yet unexplained enhancement in the octupole correlations in the ground state at deformation  $\beta_2 = 0$ . Transition strengths are overpredicted with respect to experiment, with  $B(E3; 3_1^- \rightarrow 0_1^+) = 41.3$  W.u. and  $B(E2; 2_1^+ \rightarrow 0_1^+) = 14.3$  W.u. Spectroscopic quadrupole moments, on the other hand, are underpredicted, with  $Q_s(3_1^-) = -0.104 \ e \text{ b} \text{ and } Q_s(2_1^+) = -0.117 \ e \text{ b}.$  We note that similar calculations were performed in Ref. [42]. The calculations presented here differ in the choice of interaction and in the fact that we do not perform a phenomenological quenching of excitation energy. The calculations of Ref. [42] yield  $B(E2; 2_1^+ \to 0_1^+) = 5.5$  W.u. and  $B(E3; 3_1^- \rightarrow 0_1^+) = 21.9 \text{ W.u.}, \text{ but do not report values}$ for  $Q_s(2_1^+)$  or  $Q_s(3_1^-)$ . Using one dimensional generator coordinate method calculations with intrinsic wave functions (i.e., no projection) one can also estimate the excitation energies and transition strengths for the 2<sup>+</sup> and 3<sup>-</sup> states, using  $\beta_2$  and  $\beta_3$ , respectively, as coordinates. The  $2^+$  state appears at 7.03 MeV with  $B(E2; 2_1^+ \rightarrow 0_1^+) =$ 4.13 W.u. On the other hand [46] the 3<sup>-</sup> level appears at 4.01 MeV with  $B(E3; 3_1^- \to 0_1^+) = 7.7$  W.u. The lower value of the excitation energies, as compared to the projected calculation, confirms the unexpectedly large stretching of excitation energies arising from the angular momentum projection and exacerbated in the spherical system. The low transition strengths in the intrinsic calculation are due to the unsuitable use of the rotational formula to connect multipole moments and transition strengths in a spherical system [47]. In the projected calculation, transition strengths are computed exactly and there is no need for approximation.

Finally, we calculate excitation spectra from Skyrme density functionals in RPA and TDHF calculations, which produce consistent results. Using the SKX interaction [48],  $E(2_1^+)=4.08$  MeV with  $B(E2;2_1^+\rightarrow 0_1^+)=6.26$  W.u. The SkM\* interaction [49] yields  $E(2_1^+)=4.79$  MeV with  $B(E2;2_1^+\rightarrow 0_1^+)=8.82$  W.u. The RPA can also be used to predict the properties of the  $3_1^-$  state. Using the SKX interaction,  $E(3_1^-)=2.619$  MeV with  $B(E3;3_1^-\rightarrow 0_1^+)=30.45$  W.u., while the SkM\* interaction gives  $E(3_1^-)=3.301$  MeV with  $B(E3;3_1^-\rightarrow 0_1^+)=33.78$  W.u. The results obtained using the SKX interaction are in a better agreement with the experimental data in terms of the excitation energies and transition probabilities.

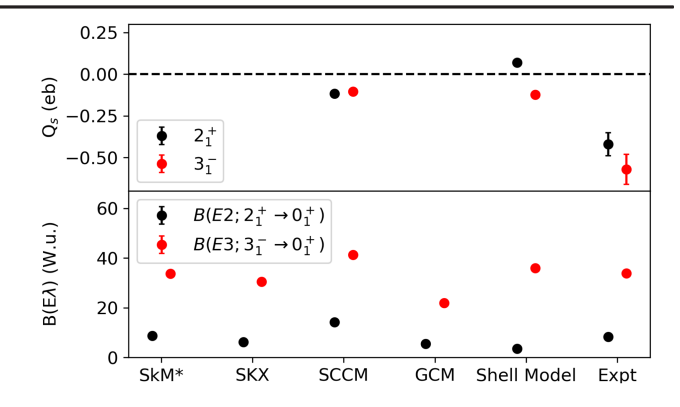


FIG. 3. Spectroscopic quadrupole moments  $(Q_s)$  and electric transition strengths  $[B(E\lambda)]$  for the  $2_1^+$  and  $3_1^-$  states studied in the present work. Shown for comparison are the HF + RPA calculations using the Skyrme-type SkM\* and SKX functionals, calculations using the SkM\* and SKX functionals, symmetry-conserving configuration mixing (SCCM) calculations, and shell-model calculations, as well as the results using the generator coordinate method (GCM) based on a covariant energy density functional by Yao and Hagino in Ref. [42].  $B(E\lambda)$  uncertainties are smaller than the symbol size.

A comparison of all experimental and theoretical data for the states of interest is presented in Fig. 3. Interestingly, both SCCM and shell-model results predict similar behavior for the  $3_1^-$  state, with a modest, negative  $Q_s(3^-)$  value and a  $B(E3; 3_1^- \to 0_1^+)$  strength of comparable magnitude to that observed in experiment. In this work we find an experimental  $Q_s(3^-)$  moment that is considerably larger in absolute terms than either calculated value. This indicates a stronger quadrupole coupling to the octupole deformed state than either model predicts. This would point to a more extended collective wave function than observed in Fig. 4(c) with respect to the quadrupole degree of freedom, and with a

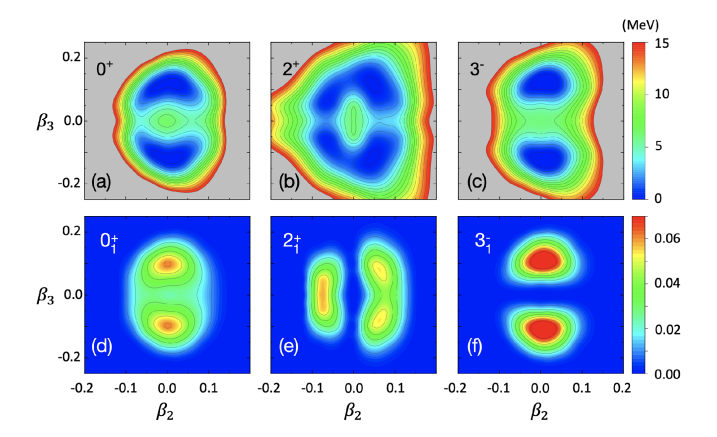


FIG. 4. Total energy surfaces for the angular-momentum projected (a)  $0^+$ , (b)  $2^+$ , and (c)  $3^-$  states in  $^{208}\text{Pb}$  calculated with the SCCM method described in the text. The collective wave functions for the  $0^+_1$ ,  $2^+_1$ , and  $3^-_1$  states are shown in (d), (e), and (f), respectively.

more prolate-dominant form. The  $B(E3; 3_1^- \rightarrow 0_1^+)$  strength, on the other hand, is approximately consistent with experiment in its magnitude.

The clearest discrepancy between theories and experiment is found in the behavior of the  $2_1^+$  state. Both shellmodel and SCCM predict a relatively small absolute  $Q_s(2^+)$  value, whereas the experiment indicates the presence of a large, negative moment. The shell model significantly underpredicts the  $B(E2; 2_1^+ \rightarrow 0_1^+)$  value as well. In general, the failure of the shell model to reproduce E2 properties can be understood from the limited mp - mhexcitations included in the calculation, which are well known to be essential to reproduce quadrupole effects. The inability of the SCCM values to reproduce the relative  $B(E2; 2_1^+ \rightarrow 0_1^+)$  and  $Q_s(2^+)$  behavior is more surprising. While the overprediction of the  $B(E2; 2_1^+ \rightarrow 0_1^+)$  strength can be understood from deficiencies in the model, described earlier, the relative behavior of the two observables might be expected to be more reliable. In Fig. 4(e), the collective wave function for the  $2_1^+$  state can be seen to be an admixture of two components, with both oblate ( $\beta_2 < 0$ ) and prolate ( $\beta_2 > 0$ ) contributions. The present experimental work implies that the prolate contribution to this state, contributing *negatively* to the quadrupole moment, is stronger than predicted in the SCCM calculations and the amplitude of the oblate component is too strong. The sign of  $\beta_2$  was then monitored in the Skyrme TDHF calculations, which reproduce both excitation energies and transition strengths. While  $Q_s$  values cannot be extracted from the model, the time average of the deformation was found to be zero, with no preference for prolate or oblate deformation. Thus, within the scope of the model, there was no indication of the stronger prolate contribution to the  $2^+_1$  state posited above. Qualitatively, however, this prolate dominance appears to be reproduced in the collective wave functions calculated in Ref. [42], with a predominantly prolate configuration for the  $2_1^+$  state and a more extended prolate wave function for the  $3_1^-$  level.

Importantly, the presently measured  $Q_s(3_1^-)$  moment is expected [20] to have implications for the splitting between the energies of the states in the two octupole-phonon quartet in <sup>208</sup>Pb. Using the approximate relation for the splitting of the two-phonon states presented in Ref. [20] suggests a splitting of between 800 and 1500 keV between the  $J^{\pi} = 0^+, 2^+, 4^+$ , and  $6^+$  states due to the coupling of quadrupole and octupole modes. As previously mentioned, a candidate has been identified for the 0<sup>+</sup> member of this quartet, lying at 5241 keV. Within the model presented in Ref. [20], the splitting required to reproduce this excitation energy would imply no coupling between octupole and quadrupole modes. This observed 0<sup>+</sup> state viewed alongside the present result thus presents something of a puzzle. Either the model presented in Ref. [20] is not appropriate, or there exists some phenomenon providing a near-exact cancellation of the implied splitting.

In conclusion, we present a state-of-the-art Coulomb-excitation study of the heaviest known doubly magic nucleus,  $^{208}$ Pb. Thanks to the experimental sensitivity, we are able to conclusively demonstrate the large, negative spectroscopic quadrupole moments of both the  $3_1^-$  and  $2_1^+$  states, as well as their consistent magnitudes. These results are indicative of a time-averaged prolate deformation for the system. As with previous attempts to calculate the  $Q_s(3_1^-)$  [50–52] moment, sophisticated contemporary nuclear models fail to reproduce both the sign and magnitude of the quadrupole moments for both the  $2_1^+$  and  $3_1^-$  states. Thus, even as a cornerstone of the nuclear landscape,  $^{208}$ Pb remains a puzzle for nuclear structure theories.

Acknowledgments—The authors thank the beam-delivery team at the ATLAS facility of Argonne National Laboratory for providing the beams. Work at the University of Surrey was supported under UKRI Future Leaders Fellowship Grant No. MR/T022264/1. Work at the University of Surrey was supported under the Science and Technologies Facilities Council (STFC) under Grant No. ST/V001108/1. Work at the University of Liverpool was supported by STFC. Work was supported by the NSF under Grants No. PHY-2208137, No. PHY-2011890, No. PHY-1913028, and No. PHY-2110365. Work of Argonne National Laboratory was supported by the U.S. Department of Energy, Office of Science, Office of Nuclear Physics, under Contract No. DE-AC02-06CH11357. Work at Lawrence Livermore National Laboratory was performed under the auspices of the U.S. Department of Energy under Contract No. DE-AC52-07NA27344. Work at UNC is sponsored by the U.S. Department of Energy under Grants No. DE-FG02-97ER41041 (UNC) and No. DE-FG02-97ER41033 (TUNL). Los Alamos National Laboratory is operated by Triad National Security, LLC, for the National Nuclear Security Administration of the U.S. Department of Energy (Contract No. 89233218CNA000001). Work was supported under U.S. Department of Energy under Contract No. DE-SC0021243. This material is based upon work supported by the U.S. Department of Energy, Office of Science, Office of Nuclear Physics, under Contract No. DEAC02-05CH11231 (LBNL). GRETINA was funded by the U.S. DOE, Office of Science, Office of Nuclear Physics, and operated by the ANL and LBNL contract numbers above. This research uses resources of ANL's ATLAS facility, which is a U.S. Department of Energy Office of Science User facility. Work was supported by the National Science Centre, Poland under Grant No. 2023/50/E/ST2/00621.

<sup>[1]</sup> M. G. Mayer, On closed shells in nuclei. II, Phys. Rev. **75**, 1969 (1949).

<sup>[2]</sup> O. Haxel, J. H. D. Jensen, and H. E. Suess, On the "magic numbers" in nuclear structure, Phys. Rev. **75**, 1766 (1949).

- [3] E. Caurier, G. Martínez-Pinedo, F. Nowacki, A. Poves, and A. P. Zuker, The shell model as a unified view of nuclear structure, Rev. Mod. Phys. 77, 427 (2005).
- [4] T. Otsuka, A. Gade, O. Sorlin, T. Suzuki, and Y. Utsuno, Evolution of shell structure in exotic nuclei, Rev. Mod. Phys. 92, 015002 (2020).
- [5] J. J. Cowan, C. Sneden, J. E. Lawler, A. Aprahamian, M. Wiescher, K. Langanke, G. Martínez-Pinedo, and F.-K. Thielemann, Origin of the heaviest elements: The rapid neutron-capture process, Rev. Mod. Phys. 93, 015002 (2021).
- [6] S. Abrahamyan *et al.* (PREX Collaboration), Measurement of the neutron radius of <sup>208</sup>Pb through parity violation in electron scattering, Phys. Rev. Lett. **108**, 112502 (2012).
- [7] D. Adhikari *et al.* (PREX Collaboration), Accurate determination of the neutron skin thickness of <sup>208</sup>Pb through parity-violation in electron scattering, Phys. Rev. Lett. **126**, 172502 (2021).
- [8] A. Trzcińska, J. Jastrzębski, P. Lubiński, F. J. Hartmann, R. Schmidt, T. von Egidy, and B. Kłos, Neutron density distributions deduced from antiprotonic atoms, Phys. Rev. Lett. 87, 082501 (2001).
- [9] J. Zenihiro, H. Sakaguchi, T. Murakami, M. Yosoi, Y. Yasuda, S. Terashima, Y. Iwao, H. Takeda, M. Itoh, H. P. Yoshida, and M. Uchida, Neutron density distributions of  $^{204,206,208}$ Pb deduced via proton elastic scattering at  $E_p = 295$  mev, Phys. Rev. C **82**, 044611 (2010).
- [10] C. M. Tarbert *et al.* (Crystal Ball at MAMI and A2 Collaborations), Neutron skin of <sup>208</sup>Pb from coherent pion photoproduction, Phys. Rev. Lett. **112**, 242502 (2014).
- [11] F. J. Fattoyev, J. Piekarewicz, and C. J. Horowitz, Neutron skins and neutron stars in the multimessenger era, Phys. Rev. Lett. 120, 172702 (2018).
- [12] P.-G. Reinhard, X. Roca-Maza, and W. Nazarewicz, Combined theoretical analysis of the parity-violating asymmetry for <sup>48</sup>Ca and <sup>208</sup>Pb, Phys. Rev. Lett. **129**, 232501 (2022).
- [13] E. Yüksel and N. Paar, Implications of parity-violating electron scattering experiments on <sup>48</sup>Ca (CREX) and <sup>208</sup>Pb (PREX-II) for nuclear energy density functionals, Phys. Lett. B **836**, 137622 (2023).
- [14] B. T. Reed, F. J. Fattoyev, C. J. Horowitz, and J. Piekarewicz, Implications of PREX-2 on the equation of state of neutron-rich matter, Phys. Rev. Lett. 126, 172503 (2021).
- [15] B. Hu, W. Jiang, T. Miyagi, Z. Sun, A. Ekström, C. Forssén, G. Hagen, J. D. Holt, T. Papenbrock, S. R. Stroberg, and I. Vernon, Ab initio predictions link the neutron skin of <sup>208</sup>Pb to nuclear forces, Nat. Phys. 18, 1196 (2022).
- [16] K. Heyde and J. L. Wood, Shape coexistence in atomic nuclei, Rev. Mod. Phys. **83**, 1467 (2011).
- [17] A. Poves, F. Nowacki, and Y. Alhassid, Limits on assigning a shape to a nucleus, Phys. Rev. C **101**, 054307 (2020).
- [18] D. Goutte, J. B. Bellicard, J. M. Cavedon, B. Frois, M. Huet, P. Leconte, P. X. Ho, S. Platchkov, J. Heisenberg, J. Lichtenstadt, C. N. Papanicolas, and I. Sick, Determination of the transition charge density of the octupole vibration in <sup>208</sup>Pb, Phys. Rev. Lett. 45, 1618 (1980).
- [19] NNDC *et al.*, Evaluated Nuclear Structure Data File (ENSDF), 10.18139/nndc.ensdf/1845010.

- [20] A. Bohr and B. R. Mottelson, *Nuclear Structure* (Benjamin, New York, 1975), Vol. 2, pp. 45, 569–570.
- [21] J. Blomqvist, The  $3^- \times 3^-$  two-phonon quartet and the proton pairing vibration in <sup>208</sup>Pb, Phys. Lett. **33B**, 541 (1970)
- [22] R. Spear, W. Vermeer, M. Esat, J. Kuehner, A. Baxter, and S. Hinds, An improved determination of the quadrupole moment of the first excited state of <sup>208</sup>Pb, Phys. Lett. **128B**, 29 (1983).
- [23] K. Vetter *et al.*, Fragmentation of the two-phonon octupole vibrational states in <sup>208</sup>Pb, Phys. Rev. C 58, R2631 (1998).
- [24] M. Yeh, P. E. Garrett, C. A. McGrath, S. W. Yates, and T. Belgya, Two-phonon octupole excitation in <sup>208</sup>pb, Phys. Rev. Lett. 76, 1208 (1996).
- [25] M. Yeh, M. Kadi, P. E. Garrett, C. A. McGrath, S. W. Yates, and T. Belgya, Candidates for two-phonon octupole excitations in <sup>208</sup>Pb, Phys. Rev. C **57**, R2085 (1998).
- [26] B. Pritychenko, M. Birch, B. Singh, and M. Horoi, Tables of E2 transition probabilities from the first 2<sup>+</sup> states in eveneven nuclei, At. Data Nucl. Data Tables **107**, 1 (2016).
- [27] A. R. Barnett and W. R. Phillips, Coulomb excitation and reorientation of the octupole state in <sup>208</sup>Pb, Phys. Rev. 186, 1205 (1969).
- [28] A. M. R. Joye, A. M. Baxter, M. P. Fewell, D. C. Kean, and R. H. Spear, Quadrupole moment of the first 3<sup>-</sup> state in <sup>208</sup>Pb, Phys. Rev. Lett. **38**, 807 (1977).
- [29] W. J. Vermeer, M. T. Esat, J. A. Kuehner, R. H. Spear, A. M. Baxter, and S. Hinds, Coulomb excitation of the 2.615 MeV (3<sup>+</sup>) and 4.086 MeV (2<sup>+</sup>) states of <sup>208</sup>Pb, Aust. J. Phys. **37**, 123 (1984).
- [30] P. Lesser, D. Cline, P. Goode, and R. Horoshko, Static electric quadrupole moments of the first excited states of <sup>56</sup>Fe and the even titanium nuclei, Nucl. Phys. **A190**, 597 (1972).
- [31] S. Paschalis *et al.*, The performance of the gamma-ray energy tracking in-beam nuclear array GRETINA, Nucl. Instrum. Methods Phys. Res., Sect. A **709**, 44 (2013).
- [32] C. Wu, D. Cline, A. Hayes, R. Flight, A. Melchionna, C. Zhou, I. Lee, D. Swan, R. Fox, and J. Anderson, CHICO2, a two-dimensional pixelated parallel-plate avalanche counter, Nucl. Instrum. Methods Phys. Res., Sect. A 814, 6 (2016).
- [33] T. Czosnyka, D. Cline, and C. Y. Wu, Bull. Am. Phys. Soc. 28, 745 (1983).
- [34] J. Henderson, https://github.com/jhenderson88/GOSIA Fitter.
- [35] M. Zielińska, L. P. Gaffney, K. Wrzosek-Lipska, E. Clément, T. Grahn, N. Kesteloot, P. Napiorkowski, J. Pakarinen, P. Van Duppen, and N. Warr, Analysis methods of safe coulomb-excitation experiments with radioactive ion beams using the GOSIA code, Eur. Phys. J. A 52, 99 (2016).
- [36] See Supplemental Material at http://link.aps.org/supplemental/10.1103/PhysRevLett.134.062502 for gammaray yields, level-schemes used in the present work and details of the theoretical calculations, which includes Refs. [37–39].
- [37] J. Berger, M. Girod, and D. Gogny, Time-dependent quantum collective dynamics applied to nuclear fission, Comput. Phys. Commun. **63**, 365 (1991).
- [38] L. M. Robledo, T. R. Rodríguez, and R. R. Rodríguez-Guzmán, Mean field and beyond description of nuclear

- structure with the Gogny force: A review, J. Phys. G 46, 013001 (2019).
- [39] G. Colò, L. Cao, N. Van Giai, and L. Capelli, Self-consistent RPA calculations with Skyrme-type interactions: The Skyrme\_rpa program, Comput. Phys. Commun. **184**, 142 (2013).
- [40] J. Heisenberg, J. Lichtenstadt, C. N. Papanicolas, and J. S. McCarthy, Excitation of low lying natural parity levels in <sup>208</sup>Pb by inelastic electron scattering, Phys. Rev. C 25, 2292 (1982).
- [41] J. Enders, P. von Brentano, J. Eberth, A. Fitzler, C. Fransen, R.-D. Herzberg, H. Kaiser, L. Käubler, P. von Neumann Cosel, N. Pietralla, V. Ponomarev, A. Richter, R. Schwengner, and I. Wiedenhöver, Nuclear resonance fluorescence experiments on <sup>204,206,207,208</sup>Pb up to 6.75 MeV, Nucl. Phys. A724, 243 (2003).
- [42] J. M. Yao and K. Hagino, Anharmonicity of multioctupole-phonon excitations in <sup>208</sup>Pb: Analysis with multireference covariant density functional theory and sub barrier fusion of <sup>16</sup>O + <sup>208</sup>Pb, Phys. Rev. C **94**, 011303(R) (2016)
- [43] B. A. Brown, Double-octupole states in <sup>208</sup>Pb, Phys. Rev. Lett. **85**, 5300 (2000).
- [44] V. Karayonchev, M. Stoyanova, G. Rainovski, J. Jolie, A. Blazhev, M. Djongolov, A. Esmaylzadeh, C. Fransen, K. Gladnishki, L. Knafla, D. Kocheva, L. Kornwebel,

- J.-M. Régis, G. De Gregorio, and A. Gargano, Lifetimes and structures of low-lying negative-parity states of <sup>209</sup>Po, Phys. Rev. C **103**, 044309 (2021).
- [45] R. N. Bernard, L. M. Robledo, and T. R. Rodríguez, Octupole correlations in the <sup>144</sup>Ba nucleus described with symmetry-conserving configuration-mixing calculations, Phys. Rev. C **93**, 061302(R) (2016).
- [46] L. M. Robledo and G. F. Bertsch, Global systematics of octupole excitations in even-even nuclei, Phys. Rev. C 84, 054302 (2011).
- [47] L. M. Robledo and G. F. Bertsch, Electromagnetic transition strengths in soft deformed nuclei, Phys. Rev. C 86, 054306 (2012)
- [48] B. A. Brown, New Skyrme interaction for normal and exotic nuclei, Phys. Rev. C 58, 220 (1998).
- [49] J. Bartel, P. Quentin, M. Brack, C. Guet, and H.-B. Håkansson, Towards a better parametrisation of Skyrmelike effective forces: A critical study of the SkM force, Nucl. Phys. **A386**, 79 (1982).
- [50] P. Ring and J. Speth, Nuclear structure calculations with a density-dependent force in <sup>208</sup>Pb, Nucl. Phys. A235, 315 (1974).
- [51] B. Sørensen, Static quadrupole moment of the collective octupole vibration in <sup>208</sup>Pb, Phys. Lett. **35B**, 101 (1971).
- [52] I. Hamamoto, Nuclear octupole vibrations in the isotopes of Pb, Nucl. Phys. A155, 362 (1970).